Relationship between resistive switching characteristics and band diagrams of Ti/$Pr_{1-x}Ca_xMnO_3$ junctions

S. Asanuma and H. Akoh
National Institute of Advanced Industrial Science and Technology (AIST), Tsukuba, Ibaraki 305-8562, Japan and Japan Science and Technology Agency (JST), CREST, Kawaguchi 332-0012, Japan

H. Yamada and A. Sawa
National Institute of Advanced Industrial Science and Technology (AIST), Tsukuba, Ibaraki 305-8562, Japan
(Received 23 July 2009; revised manuscript received 29 October 2009; published 8 December 2009)

We investigated the Ca-composition dependence of the resistive switching (RS) characteristics and band diagrams in Ti/$Pr_{1-x}Ca_xMnO_3$ [PCMO(x)] junctions and the impact of oxygen vacancies on the band diagrams. Hysteretic current-voltage characteristics, i.e., the RS effect, were observed for Ti/PCMO(x) junctions with $x<0.8$, whereas junctions consisting of n-type semiconducting PCMO(x) with $x>0.8$ showed almost no RS effect. The RS ratio R_H/R_L, where R_H and R_L are resistances of high- and low-resistance states, respectively, showed a clear x dependence: R_H/R_L increased with increasing x and was maximized at $x\sim0.4$. Cross-sectional transmission electron microscope images of the switched Ti/PCMO(x) junctions confirmed the formation of amorphous TiO_y layers at the interfaces. Electron energy-loss measurements of the Mn-L edge indicated that oxygen-deficient PCMO(x) layers were formed at the interface due to the electrochemical migration of oxygen ions. Optical-absorption measurements of oxygen-deficient PCMO(x) films revealed that the formation of oxygen vacancies increased the band gap of PCMO(x). On the basis of the results, we propose a possible model involving the change in barrier height and/or width for the hole-carrier conduction at the PCMO(x) interface induced by the electrochemical migration of oxygen vacancies as the mechanism of the RS effect.

DOI: 10.1103/PhysRevB.80.235113 PACS number(s): 73.40.−c, 73.30.+y, 73.20.−r

I. INTRODUCTION

Currently, resistance random access memory based on hysteretic resistive switching (RS) in transition-metal oxides (TMOs) is considered a promising candidate for high-density nonvolatile memory. The RS effect has been observed in capacitorlike structures containing various semiconducting and insulating TMOs, such as $Pr_{0.7}Ca_{0.3}MnO_3$ (PCMO),[1–7] Cr-doped $SrZrO_3$,[8] Cr-doped $SrTiO_3$,[9] NiO,[10–12] TiO_2,[13,14] Cu_2O,[15] and CoO,[16,17] sandwiched between two metal electrodes, and the observed RS behaviors differ depending on the oxides and/or combinations of oxide and electrode metal. The variety of RS behaviors suggests that there may be some different types of mechanisms involved in the RS effect.

To understand the mechanisms involved, classifications of the RS behaviors have been proposed.[18,19] In terms of current-voltage (I-V) characteristics, the RS behavior can be classified into two types: unipolar and bipolar. In addition to this classification, the conducting path is also used to categorize the RS behaviors. One type of conducting path is a filament-type path in which the resistive switching originates from the formation and rupture of conductive filaments in an insulating matrix.[11–13,20] Thermal redox and/or electrochemical migration of oxygen vacancies have been considered to be the mechanism for the formation and rupture of the filaments. The other type of conducting path is an interface-type path, in which RS takes place at the interface between a metal electrode and an oxide. The interface-type RS has been observed in semiconducting perovskite oxides, such as $Pr_{0.7}Ca_{0.3}MnO_3$ and Nb-doped $SrTiO_3$.[3,6,21–23] Concerning the driving mechanism, recent studies have indicated that the electrochemical migration of oxygen vacancies induces the RS effect.[7,19,24–26] However, the impact of the oxygen vacancies on the electronic structure and/or the band diagram in controlling the electrical conduction process is still poorly understood.

In this paper, we report the relationship between the RS characteristics and the band diagrams of Ti/$Pr_{1-x}Ca_xMnO_3$ [PCMO(x)] junctions and the impact of oxygen vacancies on the band diagrams. PCMO(x), particularly $x=0.3$, is one of the typical materials showing the interface-type RS effect.[3,6,24] Since PCMO(x) is a correlated electron oxide, the electronic structure changes with carrier concentration, i.e., Ca composition x.[27] If PCMO(x) itself is responsible for the RS effect, a change in the electronic structure of PCMO(x) may affect the RS characteristics. This study has revealed that the RS characteristics of Ti/PCMO(x) junctions depended on the Ca composition x, and that junctions with $x>0.8$ showed almost no RS effect. Moreover, we found that oxygen vacancies were formed in the PCMO(x) layer in the vicinity of the interface by applying an electric field, and that the formation of oxygen vacancies increased the band gap of PCMO(x). On the basis of our experimental results, we describe possible band diagrams of the Ti/PCMO(x) interfaces in high- and low-resistance states and discuss a possible model of the RS effect based on these band diagrams.

The paper is organized as follows. In Sec. II, we present the Ca composition, x, dependence of the RS characteristics of Ti/PCMO(x) junctions and the structural properties of Ti/PCMO(x) interfaces. In Sec. III, we discuss the band diagrams of PMCO(x) and the impact of oxygen vacancies on the band diagrams. In Sec. IV, we propose a possible model

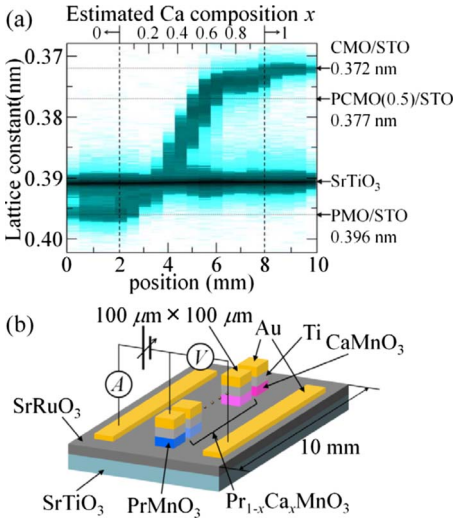

FIG. 1. (Color online) (a) Out-of-plane lattice constant of Ca-composition-spread epitaxial $Pr_{1-x}Ca_xMnO_3$ [PCMO(x)] films on $SrTiO_3$ (100) substrate measured by local x-ray diffraction. Out-of-plane lattice constants of $PrMnO_3$ (PMO), $Pr_{0.5}Ca_{0.5}MnO_3$ [PCMO(0.5)], and $CaMnO_3$ (CMO) films separately deposited on STO substrates are shown on the right vertical axis. Estimated spatial change of x in the composition-spread film is shown on the upper horizontal axis (see text). (b) Schematic of the sample used for I-V measurements of Ti/PCMO(x) junctions. The real sample was 10 mm long and ~5 mm wide, containing 41 junctions with various Ca compositions.

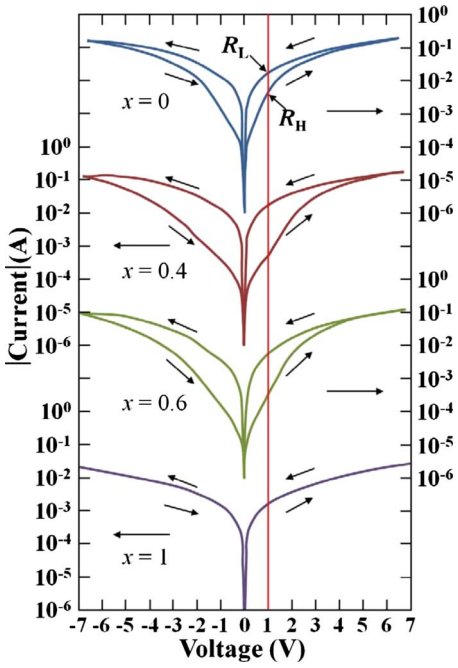

FIG. 2. (Color online) I-V characteristics of Ti/PCMO(x) junctions with x=0, 0.4, 0.6, and 1 measured at room temperature. Except for the junction with x=1, hysteretic behavior was observed for all values. R_L and R_H were determined from the current measured at V=+1 V.

of the driving mechanism based on the band diagrams of Ti/PCMO(x) interfaces. Section V gives a brief summary of the present study.

II. RS CHARACTERISTICS OF Ti/PCMO(x) JUNCTIONS

A. Sample preparation

To evaluate the carrier-concentration dependence of the RS characteristics, Ca-composition-spread PCMO(x) films with x ranging from 0 to 1 were deposited on epitaxial $SrRuO_3$ (SRO) electrodes on (100) $SrTiO_3$ (STO) substrates by a combinatorial pulsed laser deposition technique.[28] The SRO and Ca-composition-spread PCMO(x) films were deposited at 760 °C in 100 and 1 mTorr of oxygen, respectively. The thicknesses of the PCMO(x) and SRO layers were 30 and 50 nm, respectively. Local (100×1000 μm) x-ray diffraction (XRD) measurements showed that the composition-spread film was epitaxially grown for the entire range of x, which can be estimated as follows. The spatial x change of the composition-spread film was estimated by comparing the c-axis lattice constants between the composition-spread film and PCMO(x) films separately deposited on STO substrates. Figure 1(a) shows the dependence of c-axis lattice constant on Ca composition x for the composition-spread film. As shown in Fig. 1(a), the c-axis lattice constant monotonically decreased with x, indicating the formation of a solid-solution film.

After an Au(180 nm)/Ti(20 nm) top electrode was deposited on the PCMO(x)/SRO by electron-beam evaporation, the layered structure was patterned into mesa structures with dimensions 100×100 μm at intervals of 100 μm by conventional photolithography and Ar-ion milling. Figure 1(b) schematically shows the sample and the measurement circuit. I-V characteristics were measured by using a three-point probe method to determine the RS ratio (R_H/R_L), where R_H and R_L are resistance values of a high-resistance state (HRS) and a low-resistance state (LRS), respectively. The positive direction of the bias voltage was defined as the direction causing current to flow from the SRO bottom electrode layer to the Ti top electrode. It has been reported that an SRO electrode realizes Ohmic contact on PCMO(x), and the contact resistance of the PCMO(x)/SRO interface is negligibly small as compared to that of a Ti/PCMO(x) interface.[6] Thus, the contact resistance of the Ti/PCMO(x) interface dominated the measured I-V characteristics.

B. Ca-composition, x, dependence of RS characteristics

Figure 2 shows typical I-V characteristics of the Ti/PCMO(x) junctions with various Ca compositions x. Here, it is noted that these I-V characteristics are the stable ones obtained after the so-called forming process, as discussed in more detail in Ref. 6. The voltage bias is swept as $0\rightarrow+7$ V $\rightarrow0\rightarrow-7$ V $\rightarrow0$. The Ti/PCMO(x) junctions with x=0, 0.4, and 0.6 show hysteretic I-V characteristics, i.e., the RS effect, but the Ti/$CaMnO_3$ (CMO) junction (x=1) shows no hysteretic behavior. We defined the upper and lower branches of the I-V curves as the LRS and HRS, respectively. By applying positive (negative) bias stress, the HRS (LRS) is converted to the LRS (HRS).

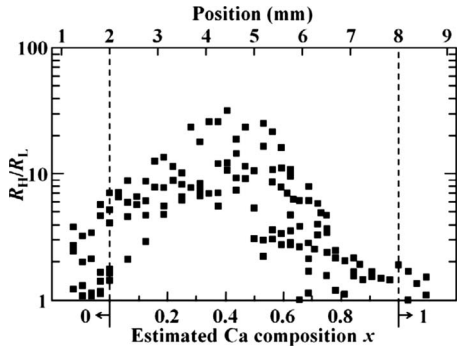

FIG. 3. Ca-composition, x, dependence of resistive switching ratio R_H/R_L measured at room temperature. R_H/R_L apparently depended on the Ca composition x, and had a maximum value (>30) at around $x=0.4$. Ti/PCMO(x) junctions with $x>0.8$ showed little change in resistance.

The RS ratios, R_H/R_L, at $V=+1$ V are plotted as a function of the Ca composition x in Fig. 3. We measured two to five junctions for each x. Although the observed values of R_H/R_L are rather scattered depending on each junction, R_H/R_L apparently depended on the Ca composition x. The RS ratio R_H/R_L increased with increasing x and showed a maximum value (>30) at around $x=0.4$. As x increased above 0.4, R_H/R_L decreased and became smaller than 2 for $x>0.8$. This Ca-composition dependence of R_H/R_L in Ti/PCMO(x) junctions is similar to the Sr composition dependence of R_H/R_L observed in Ti/$La_{1-x}Sr_{1+x}TiO_4$ [LSMO(x)] junctions, in which an atomically flat cleared surface of LSMO(x) single crystals is used.[29] In Ti/LSMO(x) junctions, the optimal Sr composition for R_H/R_L was around $x=0.5$, and the junction with $x=1$ showed no RS effect. According to these results, we suggest that a moderate hole-carrier concentration of manganites is a prerequisite for the RS effect, and also that the heavy hole doping, i.e., small number of e_g electron carriers, suppresses the RS effect.

C. Structural properties of Ti/PCMO(x) interfaces

Next, to evaluate the structural properties at Ti/PMCO(x) interfaces, cross-sectional transmission electron microscope (TEM) images of Ti/PCMO(x) junctions with different Ca compositions were observed. The Ti/PCMO junctions for TEM observations were prepared by using single-composition PCMO(x) films. Figure 4 shows cross-sectional TEM images of the Ti/PCMO(x) junctions with $x=0$, 0.5, and 1. As seen in Fig. 4(a), for the as-prepared Ti/PCMO(0.5) junction (before a switching operation), there was an amorphous TiO_y (a-TiO_y) layer with a thickness of at most 1 nm between the Ti electrode and the PCMO(0.5) layer. After applying electric fields above 5 V, the thickness of the a-TiO_y layer increased to ~10 nm, as seen in Fig. 4(b). In addition, a-TiO_y layers with a thickness of ~10 nm were formed at the Ti/PCMO(x) interfaces with both $x=0$ and 1 [Figs. 4(c) and 4(d)]. From high-resolution TEM images of these interfaces, we confirmed that the PCMO(x) layers kept the perovskite structure even after the switching

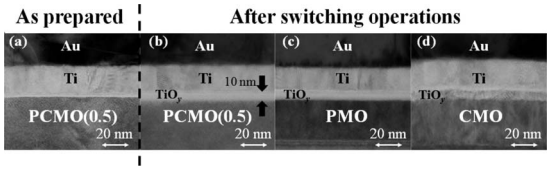

FIG. 4. Cross-sectional TEM images of Ti/PCMO(0.5) junctions observed (a) before and (b) after switching operations at room temperature. In as-prepared junctions, a thin amorphous TiO_y layer (<1 nm) was confirmed between the Ti and PCMO(0.5) layers. Switching operations (application of voltage stress) increased the thickness of the amorphous TiO_y layer to ~10 nm. After the switching operations, about 10-nm thick amorphous TiO_y layers were also observed in (c) Ti/PCMO(0) ($PrMnO_3$; PMO) and (d) Ti/PCMO(1) ($CaMnO_3$; CMO) junctions.

operations. Thus, the formation of the a-TiO_y layers may indicate that oxygen ions are diffused into the Ti electrode from the PCMO(x) layer due to the electrochemical migration process.

In order to confirm the diffusion of oxygen ions at the interface, we carried out electron energy-loss spectroscopy (EELS) measurements of the Mn-L edge. Figure 5(a) shows the electron energy-loss spectra of the Mn-L edge obtained at different positions in the PCMO(0.5) layer, as indicated in Fig. 5(b). The resistance state of the measured Ti/PCMO(0.5) junction was an HRS. As seen in Fig. 5(a), the peak intensity ratio of Mn-L_3 and Mn-L_2, $I(L_3)/I(L_2)$, decreased with increasing distance from the boundary between the a-TiO_y and the PCMO(0.5) layers. The EELS measurements of manganese oxides in Ref. 30, showing that $I(L_3)/I(L_2)$ increases as the valence of the Mn ion decreases, indicate that the valence of the Mn ion in the vicinity of the interface was smaller than that far from the interface, although the valence of the Mn ion cannot be estimated from $I(L_3)/I(L_2)$. Shono *et al.* also reported the formation of an a-TiO_y layer and reduction of the valence of the Mn ion at a Ti/PCMO(0.3) interface.[31] Since oxygen deficiencies reduce the valence of the Mn ion in PCMO(x),[32] the EELS results indicate that the number of oxygen vacancies in the vicinity of the interface was increased due to the migration of oxygen ions from the PCMO(x) layer to the Ti electrode.

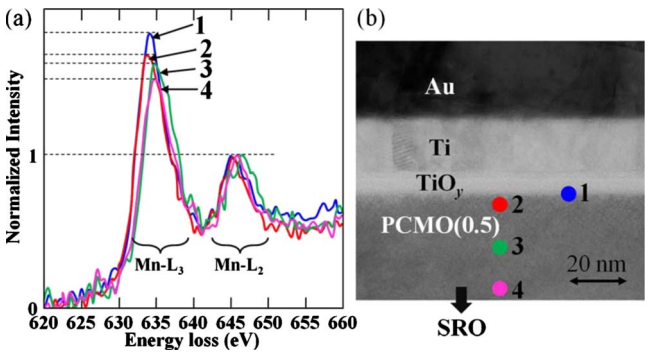

FIG. 5. (Color online) (a) Electron energy-loss spectra of Mn-L edge at several positions in Ti/PCMO(0.5) junction and (b) cross-sectional TEM image of Ti/PCMO(0.5) junction. Positions where each spectrum was measured are indicated in (b). Spectra were normalized by the intensity of the Mn-L_2 peak.

III. BAND DIAGRAMS OF PCMO(x)

A. Sample preparation

To gain a deeper understanding of the x dependence of the RS characteristics, we evaluated the band diagrams of PCMO(x), such as the band gap and the work function of PCMO(x). The band gap and the work function of PCMO(x) can be estimated from the measurements of an optical-absorption spectrum of PCMO(x) films and capacitance-voltage (C-V) characteristics of PCMO(x)/$SrTi_{0.9998}Nb_{0.0002}O_3$ (Nb:STO) junctions, respectively. For optical measurements, 40-nm-thick PCMO(x) films with $x=0$, 0.5, and 1 were deposited on STO substrates at 760 °C in 1 mTorr oxygen pressure. PCMO(x) films for the junctions were also deposited on Nb:STO substrate under the same growth conditions (Nb:STO is an n-type semiconductor which has a band gap of ~3.2 eV). An Au (200 nm) electrode was deposited on the PCMO(x)/Nb:STO, and then the Au/PCMO(x) layered structure was patterned into mesa structures with dimensions 100×100 μm.

In order to evaluate the impact of oxygen vacancies on the band diagram, we measured the optical-absorption spectra of reduced PCMO(x) films on STO substrates and the C-V characteristics of reduced PCMO(x)/Nb:STO junctions. To reduce the oxygen content of the PCMO(x) films, the films were annealed at 600 °C under ~10^{-7} Torr for 1 h. The XRD measurements confirmed that the reduced films did not decompose during the reduction process, and that c-axis lattice constants of the reduced films increased. For instance, the reduced PCMO(0.5) had a c-axis lattice constant of 0.378 nm, which was ~0.001 nm larger than that of the oxygenated ones.[33] The increase of lattice constants of the reduced films is in agreement with the result for oxygen-deficient bulk manganites.[32] Although the oxygen stoichiometry of the films cannot be estimated, the results suggest that the PCMO(x) films annealed under the above conditions have oxygen deficiencies. After the optical-absorption and C-V measurements, the samples were annealed at 600 °C in 1 atm of oxygen. Then, we measured again the optical-absorption spectra and C-V characteristics of the reoxygenated samples and confirmed that the band gap and work function of the films recovered.

B. Band gap of PCMO(x)

Optical-absorption spectra of the reduced and oxygenated PCMO(x)/STO thin films with $x=0$, 0.5, and 1 are shown in Fig. 6(a). The broken straight lines in Fig. 6(a) are drawn to fit the rising part of the absorption spectra, and the band gap can be estimated from the intersection of the broken line at the optical-absorption coefficient $\alpha=0$. The band gaps of the oxygenated PCMO(x) films were estimated to be ~0.6 eV for $x=0$, ~0.2 eV for $x=0.5$, and ~1.1 eV for $x=1$. As seen in Fig. 6(a), independently of x, the reduced PCMO(x) films, i.e., the oxygen-deficient films, had larger band gaps compared with the oxygenated ones. The increase of the band gap was estimated to be 0.2–0.4 eV. It has been reported that the formation of oxygen vacancies in Mn-O-Mn chains increases the resistivity of manganites.[32] In the present study, the resistivity of the oxygen-deficient PCMO(x) films was larger than that of the oxygenated ones. The increase of the resistivity can be attributed to the suppression of a transfer interaction of e_g-state conduction electrons between neighboring Mn sites, i.e., the reduction of the effective one-electron band width of the e_g band.[27] As a result, the band gap of the oxygen-deficient PCMO(x) may increase.

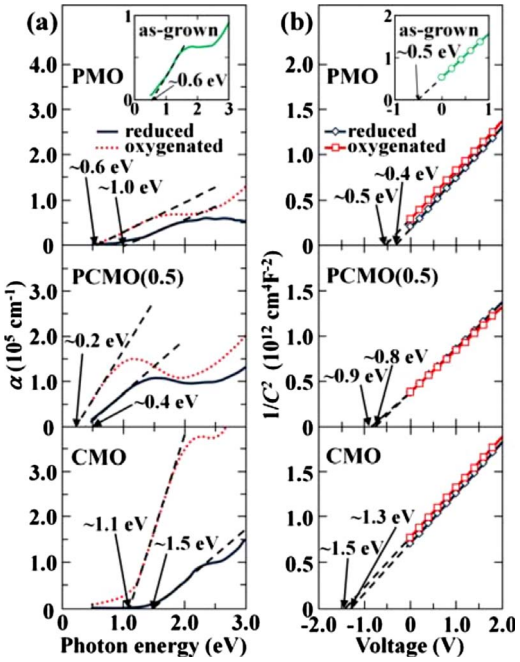

FIG. 6. (Color online) (a) Optical-absorption spectra of reduced (solid line) and oxygenated (dotted line) PCMO(x) films on STO substrates with $x=0$, 0.5, and 1 measured at room temperature. The broken straight lines are fits to the rising part of the absorption spectra, and the band gap was estimated from the intersection of the broken line at the optical-absorption coefficient $\alpha=0$. (b) $1/C^2$-V characteristics of reduced and oxygenated PCMO(x)/Nb:STO junctions with $x=0$, 0.5, and 1 measured at room temperature. The $1/C^2$-V characteristics showed a linear relationship, indicating the formation of depletion layers at the interface. Extrapolation of the straight line to $1/C^2=0$ gives the built-in potential V_{bi}. The insets of the upper panels show optical-absorption spectrum and $1/C^2$-V curve of as-grown $PrMnO_3$ (PMO) samples which were prepared separately from the samples used in the reduction and oxygenation experiments. The band gap and built-in potential of the as-grown samples are almost identical to those of the oxygenated ones.

C. Fermi level of PCMO(x)

To estimate the work functions of PCMO(x), we measured capacitance-voltage (C-V) characteristics of the PCMO(x)/Nb:STO junctions. We have previously reported that the difference of the work functions between manganites and Nb:STO, i.e., the built-in potential (eV_{bi}), can be estimated from C-V characteristics.[34,35] Since the work function of Nb:STO (ϕ_{STO}) is known to be ~3.9 eV, the work function of PCMO(x) (ϕ_{PCMO}) can be estimated to be the sum of eV_{bi} and ϕ_{STO}. Figure 6(b) shows $1/C^2$-V characteristics, with negative bias, of the oxygenated and reduced PCMO(x)/Nb:STO junctions with $x=0$, 0.5, and 1. The

PCMO(x)/Nb:STO junctions exhibited rectifying I-V characteristics (not shown), indicating the formation of a depletion layer at the interface. For a conventional semiconductor rectifying junction, $1/C^2$ versus I-V shows a linear relationship expressed by $1/C^2 \propto (V_{bi}\text{-}V)$.[36] Since the PCMO($x$)/Nb:STO junctions showed a linear relationship between $1/C^2$ and V, as seen in Fig. 6(b), we can estimate V_{bi} from the intersection of the $1/C^2$-V curve at $1/C^2=0$. The built-in potential eV_{bi} of the oxygenated PCMO(x)/Nb:STO junctions was found to be ~0.5 eV for $x=0$, ~0.9 eV for $x=0.5$, and ~1.5 eV for $x=1$. Taking the work function of Nb:STO of ~3.9 eV, the work functions of PCMO(x) for $x=0$, 0.5, and 1 were estimated to be ~4.4, ~4.8, and ~5.3 eV, respectively. This means that the Fermi level of PCMO(x) shifts downward with increasing x. The downward shift of the Fermi level is in good agreement with the chemical-potential shift of PCMO(x) films with increasing x, evaluated by photoemission spectroscopy.[37] As seen in Fig. 6(b), oxygen vacancies had an impact on the Fermi level of the PCMO(x): the Fermi levels shifted upward by 0.1–0.2 eV. The shift of the Fermi level may relate to the increase of the band gap observed in the optical-absorption measurements. In addition, the change in the carrier concentration is expected to shift the Fermi level of PCMO(x). As mentioned previously, for the carrier doping into manganites by chemical substitution, photoemission spectroscopy measurements have confirmed that the chemical potential of manganites shifts with the carrier concentration.[37–40] Because an oxygen vacancy decreases the valence of the Mn ion, the number of e_g-electron carriers increases with increasing number of oxygen vacancies. As a result, the change in the carrier concentration caused by oxygen vacancies may induce the Fermi-level shift of the PCMO(x).

D. Possible band diagrams of PCMO(x)

The type of carrier in PCMO(x) is important to describe the band diagram. It is well known that the carriers of lightly alkaline-earth-doped manganites such as $La_{1-x}Sr_xMnO_3$ and PCMO(x) are holes;[41,42] thus, lightly Ca-doped PCMO(x) can be regarded as a p-type semiconductor. On the other hand, for heavily Ca-doped manganites $Ln_{1-x}Ca_xMnO_3$ with $x \geq 0.9$ (where Ln is lanthanoid), their carriers are found to be electrons from Hall and Seebeck coefficient measurements.[43,44] In order to confirm the type of carrier in the present study, Hall measurements were carried out in PCMO(x) films at room temperature. From the magnetic field dependence of Hall resistivities shown in Fig. 7, it was confirmed that the carriers in the PCMO(x) films with $x>0.8$ were electrons, indicating that the PCMO(x) films with $x>0.8$ can be regarded as an n-type semiconductor. Note that in order to clarify at which Ca content the type of carrier of PCMO(x) changes, the Hall resistivity of the PCMO(x) films with $0.5 \leq x \leq 0.8$ was measured at room temperature. However, we could not obtain a reliable Hall resistivity of those films, because of their large carrier concentrations.

On the basis of the present experimental results, we summarized possible energetic alignments of the valence and conduction bands of the oxygenated and reduced PCMO(x) films in comparison with the Fermi level of Ti, as shown in Fig. 8. In the case of the p-type PCMO(x) with $x \leq 0.5$, the top of the valence band is located below the Fermi level of Ti. Thus, a Schottky-like barrier is expected to form at the Ti/PCMO(x) interfaces, as seen in Fig. 9(b). For the n-type PCMO(1), i.e., CMO, the bottom of the conduction band is located below the Fermi level of Ti. From this energetic alignment, we can expect that a depletion layer in the CMO does not act as an effective barrier to electron-carrier conduction at the Ti/CMO interface, as seen in Fig. 10(b).

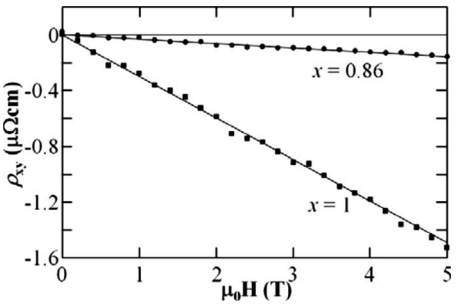

FIG. 7. Hall resistivity of PCMO(x) layers with $x=0.86$ and 1 versus magnetic field at room temperature.

IV. POSSIBLE MODEL OF THE RS EFFECT

Here, we discuss a possible model of the RS effect for the Ti/PCMO(x) interface based on the band diagrams. The TEM (Fig. 4) and the electron energy-loss (Fig. 5) experiments indicated that the oxygen vacancies (ions) migrated

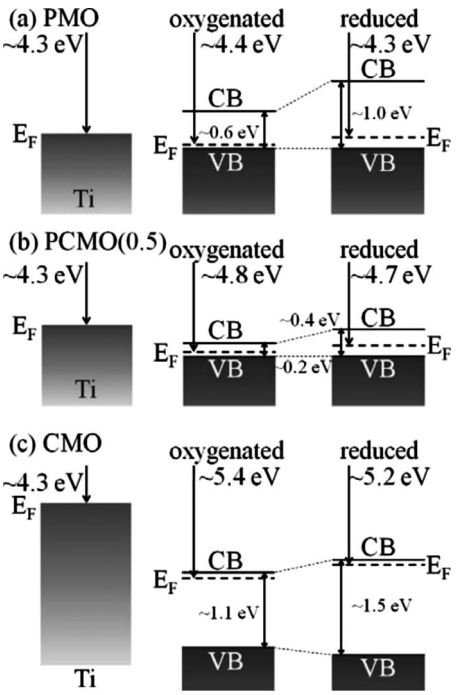

FIG. 8. Energetic alignments of conduction and valence bands of PCMO(x) layers with $x=0$, 0.5, and 1 to Fermi level of Ti. CB,VB, and E_F are the conduction band, the valence band, and the Fermi level, respectively.

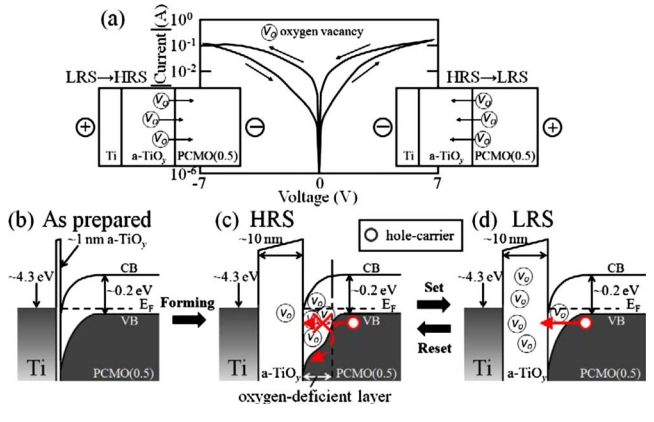

FIG. 9. (Color online) (a) Typical *I-V* characteristics of Ti/PCMO(0.5) junction. The insets in (a) illustrate schematic models of migration of oxygen vacancies depending on the polarity of an applied voltage. Possible band diagrams of Ti/PCMO(0.5) interface (b) as-prepared, (c) in a high-resistance state (HRS), and (d) in a low-resistance state (LRS). In the HRS, the oxygen-deficient PCMO(0.5) layer at the interface, having a larger band gap, acts as a barrier to hole-carrier conduction.

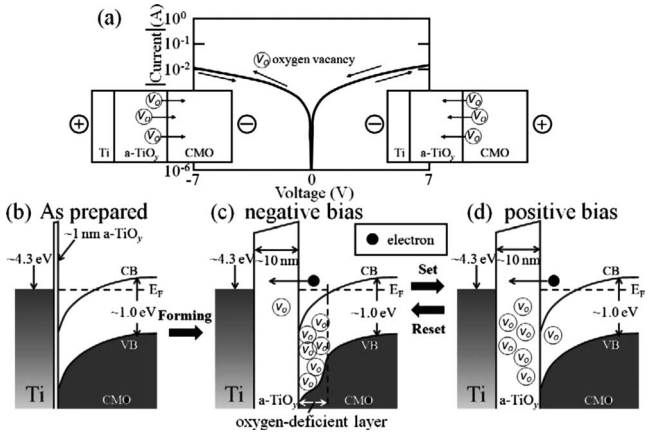

FIG. 10. (a) Typical *I-V* characteristics of Ti/CMO junction. The insets illustrate a model of migration of oxygen vacancies. Possible band diagrams of Ti/CMO interface (b) as-prepared, (c) after applying a negative voltage bias, and (d) after applying a positive voltage bias.

between the a-TiO_y layer and the PCMO(x) layer by applying voltage stresses, resulting in the change in the number of oxygen vacancies in the PCMO(x) and a-TiO_y layers. To elucidate the role of the oxygen vacancies in the RS effect, we should first understand the change in the number of oxygen vacancies between the HRS and the LRS. The direction of the oxygen-vacancy migration can be evaluated from the hysteretic *I-V* characteristics. In the Ti/PCMO(0.5) junction, when a positive voltage bias was applied to the PCMO(0.5) layer, the resistance state was converted from the HRS to the LRS, as shown in Fig. 9(a). In this case, positively charged oxygen vacancies are expected to migrate from the PCMO(0.5) layer into the a-TiO_y layer, as shown in the inset of Fig. 9(a). On the other hand, during the switching from the LRS to the HRS, oxygen vacancies are expected to diffuse into the PCMO(0.5) layer from the a-TiO_y layer. It is therefore presumable that the number of oxygen vacancies in the vicinity of the interface in the HRS is larger than in the LRS. In the HRS, the highly oxygen-deficient PCMO(0.5) layer in the vicinity of the interface has a larger band gap and could act as an effective barrier to the hole-carrier conduction, as shown in Fig. 9(c). On the other hand, because of the small number of oxygen vacancies in the PCMO(0.5) layer, the band gap at the interface decreases, and hole carriers could flow through a thin depletion layer via a tunneling process in the LRS, as shown in Fig. 9(d). Such a change in the band diagram at the interface may control the hole-carrier conduction, such as a tunneling process and thermionic emission, at the interface.

In the n-type CMO case, the TEM image shows that a-TiO_y layer is formed at the interface, indicating that oxygen ions migrated from the CMO layer to the Ti electrode. From this result, we can expect that oxygen vacancies may migrate electrochemically back and forth between the CMO layer and the a-TiO_y layer by applying a voltage of opposite polarity. When a negative voltage bias is applied to the CMO layer, a highly oxygen-deficient CMO layer may form in the vicinity of the interface and the band gap of the interface may increase, as shown in Fig. 10(c). However, since the bottom of the conduction band of the oxygen-deficient CMO layer is estimated to be below the Fermi level of the Ti electrode (Fig. 8), the change in the band gap may have little impact on the electron-carrier conduction, as shown in Figs. 10(c) and 10(d). This prediction is consistent with the experimental result that the Ti/PCMO(x) junctions with $x>0.8$ exhibited almost no RS effect.

The results of the present study suggest that the oxygen-deficient PCMO(x) layer at the interface is responsible for the RS effect of the Ti/PCMO(x) junction. However, the change in the number of oxygen vacancies in the a-TiO_y layer is also expected to cause an alteration in the resistance of the a-TiO_y layer, because TiO_2 junctions also show the RS effect.[13,14] In the model proposed above, the Ti/PCMO(x) junctions with $x>0.8$, which have electron carriers, should show no RS effect. Therefore, the small R_H/R_L (≤ 2) observed in the Ti/PCMO(x) junctions with $x>0.8$ (Fig. 3) may result from the change in the resistance of the a-TiO_y layers. In order to elucidate definitively the mechanism, further study on the contribution of the a-TiO_y layer to the RS effect is needed.

V. SUMMARY

We have studied the resistive switching (RS) characteristics at Ti/$Pr_{1-x}Ca_xMnO_3$ [PCMO(x)] junctions whose Ca composition x, i.e., carrier concentration, was systematically changed. The RS ratio showed a clear x dependence: The RS ratio increased with increasing x and had a maximum around $x=0.4$. As x was increased above 0.4, the RS ratio decreased, and the Ti/PCMO(x) junctions with $x>0.8$ showed almost no RS effect. Transmission electron microscope observations of the Ti/PCMO(x) interfaces and electron energy-loss measurements of the Mn-L edge revealed that amorphous TiO_y (a-TiO_y) layers and oxygen-deficient PCMO(x) layers were formed at the interfaces due to the electrochemical migration

of oxygen ions (vacancies). From optical-absorption spectra of the oxygen-deficient PCMO(x) films, it was found that the formation of oxygen vacancies increased the band gap of PCMO(x). Based on the experimental results, we propose that the change in the band diagram at the interface induced by the band-gap variation of PCMO(x) layer accounts for the RS effect in the Ti/PCMO(x) interface. The current study has demonstrated control of the RS characteristics by the doping level and the key role of the band diagram at the interface in the RS effect at metal-manganite junctions.

ACKNOWLEDGMENTS

The authors would like to thank Y. Tomioka of the Nanoelectronic Research Institute of AIST for useful discussions and H. Matsui and T. Hasegawa of the Photonics Research Institute of AIST for their help in the optical-absorption measurements. A.S. acknowledges the partial support of the Industrial Technology Research Grant Program in 2005 from the New Energy and Industrial Technology Development Organization (NEDO) of Japan.

[1] A. Asamitsu, Y. Tomioka, H. Kuwahara, and Y. Tokura, Nature (London) **388**, 50 (1997).
[2] S. Q. Liu, N. J. Wu, and A. Ignatiev, Appl. Phys. Lett. **76**, 2749 (2000).
[3] A. Baikalov, Y. Q. Wang, B. Shen, B. Lorenz, S. Tsui, Y. Y. Sun, Y. Y. Xue, and C. W. Chu, Appl. Phys. Lett. **83**, 957 (2003).
[4] A. Odagawa, H. Sato, I. H. Inoue, H. Akoh, M. Kawasaki, Y. Tokura, T. Kanno, and H. Adachi, Phys. Rev. B **70**, 224403 (2004).
[5] K. Aoyama, K. Waku, S. Asanuma, Y. Uesu, and T. Katsufuji, Appl. Phys. Lett. **85**, 1208 (2004).
[6] A. Sawa, T. Fujii, M. Kawasaki, and Y. Tokura, Appl. Phys. Lett. **85**, 4073 (2004).
[7] Y. B. Nian, J. Strozier, N. J. Wu, X. Chen, and A. Ignatiev, Phys. Rev. Lett. **98**, 146403 (2007).
[8] A. Beck, J. G. Bednorz, Ch. Gerber, C. Rossel, and D. Widmer, Appl. Phys. Lett. **77**, 139 (2000).
[9] Y. Watanabe, J. G. Bednorz, A. Bietsch, Ch. Gerber, D. Widmer, A. Beck, and S. J. Wind, Appl. Phys. Lett. **78**, 3738 (2001).
[10] I. G. Baek, M. S. Lee, S. Seo, M. J. Lee, D. H. Seo, D.-S. Suh, J. C. Park, S. O. Park, H. S. Kim, I. K. Yoo, U.-In Chung, and J. T. Moon, Tech. Dig. - Int. Electron Devices Meet. **2004**, 587.
[11] S. Seo, M. J. Lee, D. H. Seo, S. K. Choi, D. S. Suh, Y. S. Joung, I. K. Yoo, I. S. Byun, I. R. Hwang, S. H. Kim, and B. H. Park, Appl. Phys. Lett. **86**, 093509 (2005).
[12] K. Kinoshita, T. Tamura, M. Aoki, Y. Sugiyama, and H. Tanaka, Appl. Phys. Lett. **89**, 103509 (2006).
[13] B. J. Choi, D. S. Jeong, S. K. Kim, C. Rohde, S. Choi, J. H. Oh, H. J. Kim, C. S. Hwang, K. Szot, R. Waser, B. Reichenberg, and S. Tiedke, J. Appl. Phys. **98**, 033715 (2005).
[14] D. B. Strukov, G. S. Snider, D. R. Stewart, and R. S. Williams, Nature (London) **453**, 80 (2008).
[15] A. Chen, S. Haddad, Y. C. Wu, Z. Lan, T. N. Fang, and S. Kaza, Appl. Phys. Lett. **91**, 123517 (2007).
[16] I. H. Inoue, S. Yasuda, H. Akinaga, and H. Takagi, Phys. Rev. B **77**, 035105 (2008).
[17] H. Shima, F. Takano, H. Muramatsu, H. Akinaga, Y. Tamai, I. H. Inoue, and H. Takagi, Appl. Phys. Lett. **93**, 113504 (2008).
[18] R. Waser and M. Aono, Nature Mater. **6**, 833 (2007).
[19] A. Sawa, Mater. Today **11**, 28 (2008).
[20] K. Szot, W. Speier, G. Bihlmayer, and R. Waser, Nature Mater. **5**, 312 (2006).
[21] T. Fujii, M. Kawasaki, A. Sawa, H. Akoh, Y. Kawazoe, and Y. Tokura, Appl. Phys. Lett. **86**, 012107 (2005).
[22] T. Fujii, M. Kawasaki, A. Sawa, Y. Kawazoe, H. Akoh, and Y. Tokura, Phys. Rev. B **75**, 165101 (2007).
[23] H. Sim, H. Choi, D. Lee, M. Chang, D. Choi, Y. Son, E. H. Lee, W. Kim, Y. Park, I. K. Yoo, and H. Hwang, Tech. Dig. - Int. Electron Devices Meet. **2005**, 777.
[24] S. Tsui, A. Baikalov, J. Cmaidalka, Y. Y. Sun, Y. Q. Wang, Y. Y. Xue, C. W. Chu, L. Chen, and J. Jacobson, Appl. Phys. Lett. **85**, 317 (2004).
[25] D. J. Seong, M. Jo, D. Lee, and H. Hwang, Electrochem. Solid-State Lett. **10**, H168 (2007).
[26] M. Quintero, P. Levy, A. G. Leyva, and M. J. Rozenberg, Phys. Rev. Lett. **98**, 116601 (2007).
[27] M. Imada, A. Fujimori, and Y. Tokura, Rev. Mod. Phys. **70**, 1039 (1998).
[28] T. Fukumura, M. Ohtani, M. Kawasaki, Y. Okimoto, T. Kageyama, T. Koida, T. Hasegawa, Y. Tokura, and H. Koinuma, Appl. Phys. Lett. **77**, 3426 (2000).
[29] Y. Tokunaga, Y. Kaneko, J. P. He, T. Arima, A. Sawa, T. Fujii, M. Kawasaki, and Y. Tokura, Appl. Phys. Lett. **88**, 223507 (2006).
[30] T. Riedl, T. Gemming, and K. Wetzig, Ultramicroscopy **106**, 284 (2006).
[31] K. Shono, H. Kawano, T. Yokota, and M. Gomi, Appl. Phys. Express **1**, 055002 (2008).
[32] H. L. Ju, J. Gopalakrishnan, J. L. Peng, Q. Li, G. C. Xiong, T. Venkatesan, and R. L. Greene, Phys. Rev. B **51**, 6143 (1995).
[33] The c-axis lattice constants of the PCMO(x) films were evaluated from the (002) peaks of the films in XRD results. The XRD system (PANalytical) used in the experiments has a two-crystal monochromator and the measurement accuracy of a lattice constant is ± 0.0002 nm at diffraction angles $\theta = 45-49°$ where the (002) peak of the films appears.
[34] A. Sawa, T. Fujii, M. Kawasaki, and Y. Tokura, Appl. Phys. Lett. **86**, 112508 (2005).
[35] A. Sawa, A. Yamamoto, H. Yamada, T. Fujii, M. Kawasaki, J. Matsuno, and Y. Tokura, Appl. Phys. Lett. **90**, 252102 (2007).
[36] S. M. Sze, *Semiconductor Devices, Physics and Technology*, 2nd ed. (Wiley, New York, 2001).
[37] H. Wadati, A. Maniwa, A. Chikamatsu, I. Ohkubo, H. Kumigashira, M. Oshima, A. Fujimori, M. Lippmaa, M. Kawasaki, and H. Koinuma, Phys. Rev. Lett. **100**, 026402 (2008).
[38] A. Fujimori, A. Ino, J. Matsuno, T. Yoshida, K. Tanaka, and T. Mizokawa, J. Electron Spectrosc. Relat. Phenom. **124**, 127 (2002).

[39] J. Matsuno, A. Fujimori, Y. Takeda, and M. Takano, Europhys. Lett. **59**, 252 (2002).
[40] K. Ebata, H. Wadati, M. Takizawa, A. Fujimori, A. Chikamatsu, H. Kumigashira, M. Oshima, Y. Tomioka, and Y. Tokura, Phys. Rev. B **74**, 064419 (2006).
[41] A. Asamitsu and Y. Tokura, Phys. Rev. B **58**, 47 (1998).
[42] S. Yamada, T. Arima, H. Ikeda, and K. Takita, J. Phys. Soc. Jpn. **69**, 1278 (2000).
[43] M. Ohtaki, H. Koga, T. Tokunaga, K. Eguchi, and H. Arai, J. Solid State Chem. **120**, 105 (1995).
[44] C. Chiorescu, J. J. Neumeier, and J. L. Cohn, Phys. Rev. B **73**, 014406 (2006).